Title
Relative Roles of Energy and Momentum Fluxes in the Tropical Response to Extratropical Thermal Forcing

Journal
Journal of Climate, 34(10)

ISSN
0894-8755

Authors
Hwang, Yen-Ting
Tseng, Hung-Yi
Li, Kuan-Chen
et al.

Publication Date
2021-05-01

DOI
10.1175/jcli-d-20-0151.1

Peer reviewed

Relative roles of energy and momentum fluxes in the tropical response to extratropical thermal forcing

Yen-Ting Hwang[1*], Hung-Yi Tseng[1], Kuan-Chen Li[1,2], Sarah M. Kang[3], Yung-Jen Chen[1], and John C. H. Chiang[4],

[1]Department of Atmospheric Sciences, National Taiwan University, Taipei, Taiwan

[2]Central Weather Bureau, Taipei, Taiwan

[3]School of Urban and Environmental Engineering, Ulsan National Institute of Science and Technology, Ulsan, Korea

[4]Department of Geography, University of California, Berkeley, CA, U.S.A.

**corresponding author: ythwang@ntu.edu.tw*

Early Online Release: This preliminary version has been accepted for publication in *Journal of Climate*, may be fully cited, and has been assigned DOI 10.1175/JCLI-D-20-0151.1. The final typeset copyedited article will replace the EOR at the above DOI when it is published.

Abstract

This study investigates the transient responses of atmospheric energy and momentum fluxes to a time-invariant extratropical thermal heating in an atmospheric model coupled to an aquaplanet mixed layer ocean with the goal of understanding the mechanisms and time-scales governing the extratropical-to-tropical connection. Two distinct stages are observed in the teleconnection: (1) A decrease in the meridional temperature gradient in midlatitudes leads to a rapid weakening of the eddy momentum flux and a slight reduction of the Hadley cell strength in the forced hemisphere. (2) The subtropical trades in the forced hemisphere decrease and reduce evaporation. The resulting change to sea surface temperature leads to the development of a cross-equatorial Hadley cell, and the Intertropical Convergence Zone shifts to the warmer hemisphere. The Hadley cell weakening in the first stage is related to decreased eddy momentum flux divergence, and the response time-scale is independent of the mixed layer depth. In contrast, the time taken for the development of the cross-equatorial cell in the latter stage increase as the mixed layer depth increases. Once developed, the deep tropical cross-equatorial cell response is an order of magnitude stronger than the initial subtropical response and dominates the

Accepted for publication in *Journal of Climate*. DOI10.1175/JCLI-D-20-0151.1.

anomalous circulation. The analysis combines the momentum and energetic perspectives on this extratropical-to-tropical teleconnection and moreover shows that the subtropical circulation changes associated with the momentum budget occur with a time-scale that is distinct from the deep tropical response determined by the thermal inertia of the tropical ocean.

Accepted for publication in *Journal of Climate*. DOI 10.1175/JCLI-D-20-0151.1.

1. Introduction

Forcings in the extratropics have been observed to influence the location of tropical precipitation in modeling studies, paleo records, and 20th-century climate (e.g. Kang et al. 2008, Chiang and Bitz 2005, Broccoli et al. 2006). The energetic and the momentum perspectives offer two alternative approaches for studying the extratropical influence on Hadley circulation (Chiang and Friedman 2012, Schneider et al. 2014, Donohoe and Voigt 2017, Kang et al. 2018, Schneider and Bordoni 2008; Bordoni and Schneider 2010), but these approaches have been kept largely separate from each other in previous studies. Our goal is to combine both approaches to evaluating the transient circulation responses to an idealized perpetual extratropical thermal forcing in order to build towards a mechanistic understanding of tropical circulation responses to extratropical forcings.

The underlying principle of the energetic framework is that the Hadley circulation alters in such a way as to accommodate the interhemispheric transfer of atmospheric energy as demanded by the extratropical forcing (Kang et al. 2008). Moist static energy (MSE, $m = C_p T + gz + Lq$) in the upper troposphere is slightly larger than the near-surface atmosphere because the gravitational potential energy

Accepted for publication in *Journal of Climate*. DOI10.1175/JCLI-D-20-0151.1.

(gz) in the upper troposphere is much greater than in the near-surface atmosphere, more than compensating the larger specific heat (C_pT) and latent heat (Lq) in the low-level atmosphere. Also, eddy contribution to meridional energy transport in the tropics is usually negligible. Therefore, the total atmospheric MSE transport in tropics tends to have the opposite direction as the mass transport in the lower branch of the Hadley cell. Kang et al. (2009) define the moist stability, $\Delta m \equiv \frac{F}{v_2}$, where $F = \langle \overline{mv} \rangle$ is the vertically integrated zonal-mean meridional atmospheric energy transport and v_2 is the mass transport of the lower branch of the Hadley circulation. With this convention, the sign of Δm is positive when energy is transported in the direction of the low level flow. Hence the gross moist stability in the tropics is negative. Since the variation in gross moist stability, the amount of energy transported per unit mass transport, is usually small (Kang et al. 2009, Hill et al. 2015), the changes of energy transport are accomplished via Hadley cell adjustments. An interhemispheric contrast in the energy source tends to induce an anomalous cross-equatorial streamfunction, with the upper branch transporting the gravitational potential energy towards the hemisphere being cooled and the lower branch transporting mass and moisture towards the hemisphere being warmed. The Intertropical Convergence Zone (ITCZ) is

Accepted for publication in *Journal of Climate*. DOI10.1175/JCLI-D-20-0151.1.

expected to lie near the “energy flux equator”, where the atmospheric meridional energy flux changes sign (Kang et al. 2008; Schneider et al. 2014; Kang 2020).

This framework has been usefully applied to interpret the tropical precipitation responses to various extratropical forcings, such as imposed sea ice or ice sheet (Chiang and Bitz 2005; Cvijanovic and Chiang 2013), anthropogenic aerosol emission (Yoshimori and Broccoli 2009; Hwang et al. 2013), freshwater hosing in North Atlantic (Zhang and Delworth 2005; Broccoli et al. 2006), excessive insolation related to cloud biases in the Southern Ocean (Hwang and Frierson 2013), and forcing atmospheric models with energy flux at the surface (q-flux) (Broccoli et al. 2006; Kang et al. 2009).

Another perspective points to the importance of the interaction between Hadley circulation and eddies from a momentum perspective (Becker et al. 1997; Kim and Lee 2001; Walker and Schneider 2006; Schneider and Bordoni 2008; Bordoni and Schneider 2010). The underlying idea is that variations in midlatitude eddies result in momentum flux convergence changes in the subtropics that are compensated by changes to the tropical overturning circulation. Starting with the Reynolds-averaging inviscid momentum equation, assuming steady-state, and neglecting vertical advection and vertical eddy terms, one can obtain an approximate balance equation between eddy

Accepted for publication in *Journal of Climate*. DOI10.1175/JCLI-D-20-0151.1.

momentum flux divergence ($\bar{S}$), zonal-mean meridional advection of planetary vorticity ($f \cdot \bar{v}$), and relative vorticity ($\bar{\zeta} \cdot \bar{v}$) in the upper troposphere:

$$(f + \bar{\zeta})\bar{v} = f(1 - Ro)\bar{v} \approx \frac{1}{a\, cos^2\vartheta} \frac{\partial}{\partial\vartheta}\left(cos^2\vartheta\overline{u'v'}\right) \equiv \bar{S} \qquad (1.1)$$

where overbars $\bar{\cdot}$ indicate time mean and zonal mean. The equation suggests that the eddies play a dominant contribution to the momentum budget if the Rossby number ($Ro = -\bar{\zeta}/f$) is small.

The influence of eddy momentum flux ($\overline{u'v'}$) on the strength of Hadley cell and monsoon circulation has been reported in the statistical analyses of interannual variability (Caballero 2007; Walker and Schneider 2006), the inter-model spread of general circulation model (GCM) biases (Caballero 2008), and a series of idealized GCM experiment with changing the latitude of maximum radiative-equilibrium surface temperature (Schneider and Bordoni 2008; Bordoni and Schneider 2010).

The energetic and momentum perspectives offer independent explanations for the extratropical influence on Hadley circulation (Chiang and Friedman 2012; Kang 2020). Given a hemispheric asymmetric extratropical forcing, the energetic perspective predicts an anomalous cross-equatorial response in the deep tropics, shifting the Hadley

Accepted for publication in *Journal of Climate*. DOI10.1175/JCLI-D-20-0151.1.

cell center and displacing the ITCZ. In contrast, the momentum perspective highlights the balance between the Hadley cell strength and eddy momentum flux divergence in the subtropics, where the Rossby number is small and vertical advection of momentum flux is negligible. In order for this perspective to apply to the entire tropics, Schneider (2006) used Eq.1.1 to classify different regimes of the Hadley circulation: a momentum-conserving regime that responds directly to thermal forcing (Lindzen and Hou 1988) and a small Rossby number regime that the circulation strength is largely determined by eddies (Walker and Schneider 2006). The transition of the two regimes has been used to interpret an abrupt development of a cross-equatorial monsoonal cell (Schneider and Bordoni 2008; Bordoni and Schneider 2010).

Our goal is to deduce mechanisms for the Hadley circulation responses to extratropical forcings. There are two aspects that makes our study unique: first, we combine the analysis of both the energetic and momentum budgets in the same experimental setting, and second we analyze the transient situation in order to determine cause and effect, keeping in mind that budgets provide only diagnostic relationships. Previous studies that investigated transient responses to extratropical forcings mostly only focus on air-sea coupling feedback mechanisms and energy

Accepted for publication in *Journal of Climate*. DOI10.1175/JCLI-D-20-0151.1.

transport (e.g. Dong and Sutton 2002, Chiang and Bitz 2005, Chiang et al. 2008, Cvijanovic and Chiang 2012, Woelfle et al. 2015). On the other hand, previous studies that evaluated momentum budget (e.g. Caballero 2007, Schneider and Bordoni 2008; Bordoni and Schneider 2010) report statistical relationships between Hadley cell strength and eddy momentum flux divergence, but in such cases the causal relationship can only be assumed. Merlis et al. (2012) investigated both the angular momentum balance and energy balance in simulations with varying orbital precession and found the Hadley circulation responses to be energetically constrained. However, similar to studies focusing on the seasonal cycle, the radiative forcings are not confined to extratropics in their experiments.

We also modify the mixed layer depth in our simulations to examine what sets the time-scale of the teleconnection. Previous studies using an energetic approach reported a 1~2 year response time for wind-evaporation-sea surface temperature (SST) feedback to induce significant tropical SST and circulation changes in simulations with realistic mixed layer depth, and it has been assumed that the time-scale arises from the thermal inertia of the mixed layer (e.g. Dong and Sutton 2002, Chiang and Bitz 2005, Chiang et al. 2008, Cvijanovic and Chiang 2012, Woelfle et al. 2015). This assumption

Accepted for publication in *Journal of Climate*. DOI10.1175/JCLI-D-20-0151.1.

however discounts a potential contribution from extratropical atmospheric circulation changes independent of the mixed layer. By varying the mixed-layer depth and changing the time-scale of the teleconnection, we provide an experimental situation that further reveals the relative roles of energy and momentum to the teleconnection.

Because of the very small signal to noise ratio of the initial tropical circulation responses to extratropical thermal forcing, we decide to simplify the experimental setup by using an aquaplanet without seasonality. The setup and the detailed calculations provided in section 2 allows us to cleanly diagnose the transient evolution without the complication of the seasonal cycle or the influence of stationary eddies. We explore the equilibrium and the transient responses in both the energetic and momentum frameworks in section 3. We find that the tropical circulation responses exhibit two distinct stages: (1) an initial subtropical response that occurs rapidly and can be interpreted via the momentum perspective and (2) a deep tropical circulation adjustment that is strongly dependent on mixed layer depth and are consistent with the energetic perspective. A mechanism for the initial stage triggering the deep tropical circulation adjustments is proposed. In section 4, we summarize our findings and

Accepted for publication in *Journal of Climate*. DOI10.1175/JCLI-D-20-0151.1.

discuss the necessity for constructing a model hierarchy to systematically understand the mechanisms with various time-scales.

Accepted for publication in *Journal of Climate*. DOI10.1175/JCLI-D-20-0151.1.

2. Methods

2.1 Model setup

We use an aquaplanet version of Geophysical Fluid Dynamics Laboratory (GFDL) Atmospheric Model 2.1 (AM2.1; Anderson et al. 2004; Delworth et al. 2006) coupled with a motionless mixed layer ocean that allows thermodynamic atmosphere-ocean interactions. The horizontal resolution of the model is 2° latitude × 2.5° longitude, and the vertical resolution of the model is 24 levels. There is no seasonal cycle, a fixed surface albedo (i.e. no sea ice or snow feedback), and steady insolation is applied, varying only with latitude so that it provides the present-day Earth's annual mean insolation at all times. The insolation is computed based on an obliquity of 23.5 degrees.

2.2 Experimental design

A set of experiments is performed with prescribed extratropical thermal forcing and varying mixed layer depth. The extratropical thermal forcing is applied between 50^{o}S and 80^{o}S by directly adding a source of heat into the oceanic mixed layer energy budget equation, as specified analytically in Eq. 2.1 below and Figure 1a. Unlike Kang et al. (2008) and Kang et al. (2009), we only prescribe forcing in one hemisphere, allowing

Accepted for publication in *Journal of Climate*. DOI10.1175/JCLI-D-20-0151.1.

us to track the evolution of heating originated from one location. This forcing is representative of ocean heat uptake or ocean heat release in a changing climate, or changes in other components that would affect net radiation at the surface, such as sea ice, aerosol, and clouds. The equation of the imposed heating, denoted H, is

$$\begin{cases} H = -A\, sin\left(\frac{\phi+50°}{30°}\pi\right) & \text{For} \quad -80° < \emptyset < -50°, \\ H = 0 & \text{otherwise,} \end{cases} \qquad (2.1)$$

where A sets the maximum strength of the forcing (W m^{-2}) and $\emptyset$ is latitude in degrees. To obtain significant transient responses with limited ensemble members, we select a relatively large value of A, 60 W m^{-2}, so that a total of 2.12PW is added to the mixed layer. The imposed hemispherically asymmetric forcing is about half of the range of the earth's seasonal cycle. Indeed, the single cross-equatorial cell in the equilibrium response (Figure 1c) implies our findings may offer insights for understanding seasonal cycle transition, while not changing insolation in the tropics directly and focusing on the extratropical influence. The strong forcing, however, does raise the question of relevance of our results to climate change signals, the latter which tends to be a lot smaller in magnitude. We have performed other cases with A being 30 W m^{-2} or 10 W m^{-2}, and the equilibrium responses are qualitatively similar, albeit smaller in magnitude.

Accepted for publication in *Journal of Climate*. DOI10.1175/JCLI-D-20-0151.1.

To investigate the role of SST in setting the response time-scales, we perform cases with 50m (MLD50), 100m (MLD100), and 200m (MLD200) mixed layer depth. Since the magnitudes of the initial midlatitude temperature and wind responses depend on mixed layer depth, we set the same mixed layer depth in the forced region to 200m in all experiments and only alter the mixed layer depth elsewhere. The unrealistically deep mixed layer depths (i.e. 200m) outside the forced region allow us to cleanly separate the processes solely related to atmospheric dynamics and those involving air-sea interactions. We have additionally performed a case with observed zonal mean annual mean mixed layer depth, which amounts to about 35m in the tropics (25^{o}S~25^{o}N). The proposed two-stage responses can be also found in the case with observed mixed layer depth, with the response time-scales being similar to the case with 50m mixed layer depth.

The control case with 50m mixed layer depth and no prescribed forcing is run for 36 years. The 60 ensemble members of MLD200 cases are run for 3 years and 5 of them are extended to 48 years, reaching equilibrium around year 10. The MLD100/50 experiments are also ran for 3 years, but only 30 ensemble members are run.

2.3 Indices

Accepted for publication in *Journal of Climate*. DOI10.1175/JCLI-D-20-0151.1.

The Southern Hemisphere Hadley cell index (φ_{SH}) is defined to be the averaged mass streamfunction between 15°S~25°S at 700hPa, measuring the strength of the extreme of the Hadley circulation in the Southern Hemisphere. The cross-equatorial Hadley cell index (φ_{EQ}) is calculated by averaging the mass streamfunction between 5°S~5°N at 700hPa. The altitude 700hPa is chosen because the maximum of mass streamfunction appears in this altitude in the control climate.

The ITCZ is generally co-located with the ascending branch of Hadley circulation and is thus tightly linked with cross-equatorial circulation. Following Adam et al. (2016a), the location of ITCZ is calculated as

$$\emptyset_{ITCZ} = \frac{\int_{\emptyset_1}^{\emptyset_2} \emptyset[\cos(\emptyset)P(\emptyset)]^N d\emptyset}{\int_{\emptyset_1}^{\emptyset_2} [\cos(\emptyset)P(\emptyset)]^N d\emptyset}, \quad (2.2)$$

where N=10, $\emptyset_1 = 20°\text{S}$, $\emptyset_1 = 20°\text{N}$, and P represents the zonal mean precipitation at the latitude $\emptyset$.

Another index that is representative of the behavior of Hadley circulation is the energy flux equator, the latitude where the vertical column integrated zonal mean energy transport $\langle\overline{vm}\rangle$ vanishes (Kang et al. 2018).

Accepted for publication in *Journal of Climate*. DOI10.1175/JCLI-D-20-0151.1.

Previous studies suggested that the boundary layer cross-equatorial flow, as well as the anomalous cross-equatorial Hadley cell, are driven by cross-equatorial SST gradients (Lindzen and Nigam 1987; Chang et al. 2000; Chiang and Bitz 2005; Cvijanovic and Chiang 2013). Here we define the interhemispheric asymmetric SST index (Δ_{SST}) as the SST difference between EQ~10^{o}S and EQ~10^{o}N to measure the interhemispheric SST asymmetry in the deep tropical region.

To investigate eddy activity responses to the imposed forcing, we calculate Eliassen-Palm flux (E-P flux) in log-pressure and spherical coordinates (as in Andrews 1987):

$$\mathrm{F}^{\phi} \equiv \rho_R \cos\phi \left[\bar{u}_z \frac{\overline{v'\theta'}}{\bar{\theta}_z} - \overline{u'v'} \right]$$

$$\mathrm{F}^{z} \equiv \rho_R \cos\phi \left[\left\{ f - \frac{(\bar{u}\cos\phi)_\phi}{a\cos\phi} \right\} \frac{\overline{v'\theta'}}{\bar{\theta}_z} - \overline{u'w'} \right] \quad (2.3)$$

Here, ϕ is latitude and $z = -H\ln(p/p_R)$, where H=7.5km, p is pressure and p_R is a reference pressure. The overbar denotes zonal mean and time mean. $\rho_R = \rho_0 \exp(-Z/H)$ where ρ_0 is a constant. f is the Coriolis coefficient and subscripts ϕ, z denote partial derivatives.

Accepted for publication in *Journal of Climate*. DOI 10.1175/JCLI-D-20-0151.1.

3. Results

3.1 Equilibrium responses

We first present the equilibrium responses, calculated by averaging the last 30 years of each simulation. For all figures in this paper, only signals that are statistically significant are shown. The anomalous warming is most apparent at the heating location and extends to the tropics, shifting ITCZ southward (Figures 1b and 1d). The imposed heating decreases the meridional temperature gradient of the southern subtropics and weakens the subtropical jet in the Southern Hemisphere (defined as the latitude of the zonal wind maximum of the entire tropics, which is located around 200 hpa) (Figure 1c). In the Northern Hemisphere, surface temperature decreases slightly in the subtropics and is nearly unchanged in extratropics. The northern subtropical jet is strengthened. The temperature, precipitation, and circulation responses in Figure 1 are nearly identical in the cases with different mixed layer depth. Increasing mixed layer depth has little influence on the equilibrium responses, consistent with Kang et al. (2008). In the next two sections, we take MLD200 case as an example to demonstrate the equilibrium responses in the momentum and the energetics perspectives.

3.1.1 Equilibrium responses in the momentum perspective

Accepted for publication in *Journal of Climate*. DOI10.1175/JCLI-D-20-0151.1.

In the control case, the eddy momentum flux convergence peaks at around 40°N and 40°S (blue shading in Figure 2a, see also the climatological E-P flux in Figure 1c), where the eddy driven jets located (defined as the latitudes of maximum zonal wind at 850hPa). In the subtropics, the eddy stress, the horizontal eddy momentum flux divergence ($S \equiv \frac{1}{a\, cos^2\vartheta}\frac{\partial}{\partial\vartheta}\left(cos^2\vartheta\overline{u'v'}\right)$), is balanced by meridional advection of absolute vorticity in the upper branch of the Hadley cell, with the poleward flows in the upper branches collocated with positive S (Figure 2a; refer to Eq.1.1 for the momentum balance).

The steady-state responses of circulation and momentum fluxes in our experiments are consistent with previous studies demonstrating the influence of eddies on Hadley cell via varying insolation (Bordoni and Schneider 2008; Schneider and Bordoni 2008; Bordoni and Schneider 2010), interannual variability (Caballero 2007), or on the spread of GCMs' climatological biases (Caballero 2008). In subtropics, the variations in eddy stress are accompanied by variations in Hadley cell strength. When imposing heating in the southern extratropics, eddy stress and Hadley cells weaken in the southern tropics and strengthen in the northern tropics (compare Figures 2a and 2b or see Figure 2c for anomalies).

Accepted for publication in *Journal of Climate*. DOI10.1175/JCLI-D-20-0151.1.

3.1.2 Equilibrium responses in the energetics perspective

Driven by the uneven distribution of insolation, the atmosphere transports energy poleward in both hemispheres in the control case (black line in Figure 3a). In extratropics, eddies transport both DSE and moisture poleward. In most of the tropics, the mean meridional overturning circulation plays the main role of transporting energy away from ITCZ, with the poleward DSE transport in the upper troposphere outweighing the equatorward moisture transport near the surface (red and blue lines in Figure 3a).

The equilibrium responses of energy fluxes in Figures 3b and 3c are consistent with previous modeling studies with various extratropical forcings (Kang et al. 2008; Kang et al. 2009; Swann et al. 2011; Hwang et al. 2013; Chiang and Friedman 2012; Schneider et al. 2014) and can be understood via the energetic framework. In a stable atmosphere, the total atmospheric energy transport (or MSE transport) is in the same direction as the DSE transport but in the opposite direction to moisture transport. Responding to the imposed heating in the Southern Hemisphere, the Hadley cell transports excessive energy to the Northern Hemisphere. Both the energy flux equator and the ITCZ shift southward (Figures 1d and 3b).

Accepted for publication in *Journal of Climate*. DOI10.1175/JCLI-D-20-0151.1.

3.2 Transient responses

Figure 4 shows the evolution of SST and circulation in all three experiments during the first three years after imposing the time-invariant extratropical forcing. To allow a direct comparison with the steady-state responses in Figure 1, time slices of year 9 of the experiments when the system approaches equilibrium are plotted in the same format (in the right columns). The propagation speed of the anomalous warming depends on latitudes, with the subtropical region (~20^{o}S) warming faster than the surrounded latitudes. The dependency of propagation speed on latitudes suggests atmospheric circulation (instead of diffusive processes) playing a critical role in the teleconnection between the tropics and extratropics. Two distinct stages of the tropical meridional mass streamfunction responses are observed – a weakening centering at around 20^{o}S occurring at around month 4 for all three experiments and an anomalous cross-equatorial cell develops later. We define the start time of the first stage as the day when the change of the strength of the southern cell ($\delta\varphi_{SH}$) becomes detectable[1]. The

---

[1] Follow Deser et al. 2012, we evaluate when the ensemble mean anomalies of the targeted index first become detectable at the 95% significant level, using a 2-sided Student's t-test, where the spread is computed using the individual simulation anomalies from all ensemble members and each ensemble member's indices are assumed to be independent. A 15-day running mean is applied when plotting the

Accepted for publication in *Journal of Climate*. DOI10.1175/JCLI-D-20-0151.1.

day of the anomalous cross-equatorial cell ($\delta\varphi_{EQ}$) first becomes significant marks the start time of Stage 2. As shown in Figure 5, the time-scale for observing statistically significant weakening of the southern cell (Stage 1) is independent of mixed layer depth, whereas the time-scale for developing a statistically significant anomalous cross-equatorial cell (Stage 2) increases with mixed layer depth. Once developed, the anomalous cross-equatorial cell strengthens throughout the simulations and dominate the equilibrium responses.

In the following two sections, we take the MLD200 case as an example to demonstrate that the two distinct stages of the tropical circulation responses are driven by different mechanisms. The southern subtropical responses in the first stage can be interpreted by the momentum perspective, and the deep tropical responses in the second stage are mostly consistent with the energetic perspective.

3.2.1 Transient responses from the momentum perspective

Figure 6a shows the time series of anomalous eddy momentum divergence (i.e. eddy stress, δS) and the product of Coriolis parameter and anomalous upper-level

---

time series of individual ensemble members (in Figures 6 and 7). The smoothing has little influence on the start time quantified here.

Accepted for publication in *Journal of Climate*. DOI10.1175/JCLI-D-20-0151.1.

meridional wind ($\delta f \bar{v}$). Poleward of 15 degrees, where local Rossby number (Ro≡ $-\bar{\zeta}/f$) is smaller than 0.4, variations of eddy momentum flux divergence (δS) are mostly balanced by anomalous zonal-mean meridional advection of planetary vorticity ($\delta f \bar{v}$) (see Eq. 1.1). For example, at Stage 1, anomalous positive eddy stress (red color centering around 45$^{\mathrm{o}}$S) is balanced by anomalously positive planetary vorticity advection ($\delta f \bar{v}$, solid contours), and anomalous negative eddy stress (blue color centering around 25$^{\mathrm{o}}$S) is balanced by anomalously negative planetary vorticity advection ($\delta f \bar{v}$, dashed contours). The Coriolis parameter f is negative in Southern Hemisphere, so anomalously negative planetary vorticity advection (i.e., negative $\delta f \bar{v}$) in southern subtropics is consistent with reduced northerly in the upper level and the weakened (more positive) southern Hadley cell (Figure 6b). After entering Stage 2 and throughout the whole simulation, any variation of Hadley cell strength (demonstrated as $\delta f \bar{v}$ in the Figure 6a) poleward of 15 degrees is always accompanied by a variation of eddy stress ($\overline{\delta S}$) with the same sign.

The momentum balance does not indicate a causal relationship. Through imposing idealized forcing confined in the extratropics and investigating the transient evolutions of the responses in experiments with varying mixed layer depth, we attribute the initial

Accepted for publication in *Journal of Climate*. DOI10.1175/JCLI-D-20-0151.1.

weakening of southern Hadley cell (φ_{SH}) in Stage 1 to reduced eddy momentum flux divergence ($\bar{S}$) in the subtropics. The imposed surface heating at 50°~80°S could lead to a reduction of $\bar{S}$ in the southern subtropics via a baroclinic and a barotropic process (See Shaw et al. 2020 and the Appendix for more detailed description of the two processes). Further analyses show the baroclinic process dominates: Both the stability near the surface and the meridional temperature gradient decrease at the equatorward side of the imposed heating, reducing eddy heat flux in the climatological baroclinic zone (around 45 °S). Associated with the reduction of eddy source, poleward eddy momentum flux and its divergence ($\bar{S}$) in the subtropics also decrease (Figure A1).

Although the equilibrium responses of momentum fluxes in subtropics discussed in Section 3.1.1 fulfill the momentum balance between Hadley cell strength (φ_{SH}) and eddy stress ($\bar{S}$), our investigation of the transient evolutions suggests the equilibrium responses are distinct from Stage 1 eddy-momentum driven response in terms of latitudinal positions and strengths (compare the equilibrium responses on the right column to the Stage 1 responses on the left in Figure 6). Moreover, there is a noticeable recovery stage in between. We defer the interpretations of the recovery stage, which

Accepted for publication in *Journal of Climate*. DOI10.1175/JCLI-D-20-0151.1.

involve interactions among SST, eddy stress ($\bar{S}$), and Hadley cell strength, to the end of section 3.2.3.

Note that the signal to noise ratios of these eddy-driven responses are small. After applying a 15-day running mean to remove high frequency internal variability in individual ensemble members, the spread of anomalous eddy stress ($\overline{\delta S}$) across ensemble members still reaches 1.3×10^{-5} m/s^2, which is larger than the y-axis in Figure 6c. The spread of anomalous southern Hadley cell strength among ensemble members is also much larger compared with the change in ensemble mean. While we are able to demonstrate the existence of Stage 1 using 60 ensemble members, identifying the time-scale of Stage 1 is not possible for individual ensemble members. It remains an open question as to how the eddy-driven mechanism discussed above plays a role in individual realizations. When accessing the spread across the ensemble members, there is a statistically significant positive correlation (R=0.6) between anomalous eddy stress ($\overline{\delta S}$) and anomalous Hadley cell strength ($\delta\varphi_{SH}$) at the time the ensemble-mean responses entering Stage 1, indicating the two factors dominating the momentum balance at this stage.

3.2.2 Transient responses from the energetic perspective

Accepted for publication in *Journal of Climate*. DOI10.1175/JCLI-D-20-0151.1.

For the MLD200 case, there is no significant change in energy transport and meridional mass streamfunction in the deep tropics before month 13. The development of the cross-equatorial cell at the 2nd stage is tightly linked with the anomalous interhemispheric SST gradient in the tropics ($\delta\ \Delta_{SST}$). When the anomalous interhemispheric SST gradient in the tropics ($\delta\ \Delta_{SST}$) becomes significant (at month 13), the anomalous mass streamfunction develops and the energy flux equator shifts southward (Figures 7b and 7c). There is an approximate 3-month lag between the cross-equatorial cell and the shift of the energy flux equator. Further analysis shows a close linkage between the energy flux equator, the cross-equatorial MSE transport, and the ITCZ. The three variables all lag the anomalous mass streamfunction ($\delta\varphi_{EQ}$) by three months for the MLD200 setting (quantitative analyses not shown, but precipitation and energy flux equator responses are plotted in Figures 7a and 7d). Once they all become statistically significant, the southward shift of the energy flux equator and the anomalous cross-equatorial cell are consistent with the energetics framework.

Our transient analysis suggests that it is only when the southern tropical SST heats sufficiently and the ITCZ shifts that the extratropical energy supply can be exported to the other hemisphere across the equator (Cvijanovic and Chiang 2012). With a deeper

Accepted for publication in *Journal of Climate*. DOI10.1175/JCLI-D-20-0151.1.

mixed layer, it takes longer for the SSTs to adjust, causing Stage 2 responses to emerge with a larger lag (Figure 5). The SST gradients drive the anomalous cross-equatorial cell, and the MSE transport adjust accordingly. Wei and Bordoni (2018) and Wei and Bordoni (2020) also emphasize a crucial role of SST gradient, reporting the migration of ITCZ lagging the variation of energy flux equator during the climatological seasonal cycle. In our Stage 2 responses, both the changes in cross-equatorial cell and the meridional mean circulation component of the cross-equatorial MSE transport occur at the time when the anomalous interhemispheric SST gradient ($\delta\, \Delta_{SST}$) become statistically significant. The 3-month lag between the energy flux equator and the anomalous interhemispheric SST gradient is explained by the eddy component of the MSE transport[2].

Note that the signal-to-noise ratio of the anomalous cross-equatorial streamfunction in Stage 2 is larger than that of the anomalous southern cell strength in Stage 1 (Figure

---

[2] The eddy component dominates the meridional MSE transport right around the ITCZ region in AM2, which differs from observation. The lead-lag relationship reported here could be a result of this model bias, therefore, we only emphasize the key role of SST gradient in determining the response time-scale of the cross-equatorial cell. Echoing the take-home message in Wei and Bordoni (2018), one needs to be caution when applying the energetic framework to interpret the responses in shorter time-scales. The transient evolution of the cross-equatorial cell could be different from the transient evolution of the MSE transport.

Accepted for publication in *Journal of Climate*. DOI10.1175/JCLI-D-20-0151.1.

6b). While the time-scale of developing a cross-equatorial cell cannot be accurately quantified in a single ensemble, the characteristics of the anomalous cross-equatorial cell are detectable for all ensemble members. There is a statistically significant positive correlation (R=0.8) between the anomalous interhemispheric asymmetric SST index ($\delta\ \Delta_{SST}$) and the strength of anomalous cross-equatorial cell $\delta\varphi_{EQ}$ at the time the ensemble mean response entering Stage 2, supporting the crucial role of SST gradient. The anomalous interhemispheric SST gradient ($\delta\ \Delta_{SST}$), the strength of anomalous cross-equatorial Hadley cell ($\delta\varphi_{EQ}$), and the cross-equatorial MSE transport all strengthen with a constant rate before approaching the new equilibrium state (not shown). The equilibrium state in the right columns in Figure 7 could simply be interpreted as a fully developed response of Stage 2.

3.2.3 Connecting the two stages: the role of wind-evaporation-SST feedback

In this section, we discuss how the weakening of southern Hadley cell in Stage 1 may lead to the cross-equatorial cell in Stage 2 via the wind-evaporation-SST feedback.

Through careful inspection of the transient evolution (Figure 7) and comparison among the three experiments of different mixed layer depth (Figure 5), the time-scale for developing the cross-equatorial cell appears to be tightly linked with the

Accepted for publication in *Journal of Climate*. DOI10.1175/JCLI-D-20-0151.1.

interhemispheric SST gradient. Following Xie et al. (2010), Jia and Wu (2013), and Hwang et al. (2017), we combine the mixed layer energy budget and the linearized version of the aerodynamic bulk formula of latent heat flux

$$\rho c_p H \frac{\partial T}{\partial t} = \delta SW + \delta LW + \delta LH_{wind} + \delta LH_{SST} + \delta LH_{RH} + \delta LH_{dT} + \delta SH$$

to analyze the surface energy budget in Southern Hemisphere subtropics to explore factors influencing SST. ρ is the density of seawater, c_p is the specific heat of seawater, H is mixed layer depth, T is the mixed layer temperature (equal to the SST), and the symbols δ on the right-hand side denote anomalies, calculated as the difference of the heating experiment (at the month of interest) and the control experiment. δSW is anomalous net downward shortwave radiation, δLW is anomalous net downward longwave radiation, δSH is anomalous sensible heat flux, δLH_{wind}, δLH_{SST}, δLH_{RH}, and δLH_{dT} respectively are anomalous latent heat flux associated with changes in surface wind speed, SST, relative humidity, and the stability of the boundary layer (the difference between surface temperature and 2m air temperature).

Figure 8a suggests that changes in latent heat flux related to changes in wind speed (δLH_{wind}) is the main factor contributing to the heating tendency in southern tropics.

Accepted for publication in *Journal of Climate*. DOI10.1175/JCLI-D-20-0151.1.

This role of wind speed suggests a link between the momentum-driven Stage 1 and the energetic related Stage 2. We hypothesize that weakening of eddy stress $\bar{S}$ in Stage 1 could lead to the cross-equatorial Hadley cell through the following four steps, illustrated in Figure 9: (1) The reduction of $\bar{S}$ at the edge of the southern cell is balanced by the reduced planetary vorticity advection due to reduced poleward flow at the upper branch. (2) To satisfy momentum balance in the subtropics, the reduction of $\bar{S}$ aloft must be balanced by the reduction of friction at the surface, requiring weakened surface easterlies. Consistently, by mass continuity, the meridional component of surface wind weakens with the weaker poleward flow in the upper branch. The weakened southeasterly surface wind results in decreasing evaporation. (3) Reduced evaporation at the surface leads to increasing SST in the southern tropics, driving the cross-equatorial Hadley cell. (4) As the cross-equatorial Hadley cell strengthens, the upper branch transports energy northward. The cross-equatorial Hadley cell also leads to a subtle increase in surface wind speed and evaporation in the northern tropics, which further enhances the interhemispheric SST gradient and the cross-equatorial Hadley cell. In this view, the anomalous eddy stress $(\delta\bar{S})$ in the upper troposphere, anomalous Hadley cell in southern subtropics, and reduced evaporation are connected, supporting

Accepted for publication in *Journal of Climate*. DOI 10.1175/JCLI-D-20-0151.1.

the hypothesis linking the momentum and the energetic perspective via the wind-evaporation-SST feedback.

The large ensemble spreads in Figure 8a and Figure 6b question if the linkage between Stage 1 and Stage 2 described above explains the transition in individual ensemble members. While we cannot exclude the possibility of other mechanisms triggering the development of the cross-equatorial cell in individual ensemble members, an evaluation across the ensemble members supports our hypothesis. At the start time of Stage 2 defined from the ensemble mean, 56 out of 60 ensemble members simulate the anomalous cross-equatorial cell in the deep tropics. Among these 56 ensemble members, all but 2 exhibit an anomalously weak southern Hadley cell and surface wind speed in the southern subtropics.. The two exceptions that do not exhibit weakening of the southern Hadley cell despite having developed a cross equatorial Hadley cell anomaly had previously exhibited an extended period with a weakened southern Hadley cell. This suggest that while it is difficult to pinpoint the onset of stage 1 in and individual integration, it appears that if the Southern Hadley cell weakens over some suitable integration period, it may be enough to initiate stage 2.

Accepted for publication in *Journal of Climate*. DOI10.1175/JCLI-D-20-0151.1.

A closer examination reveals that, before the anomalous cross-equatorial cell fully develops and the southern Hadley cell almost diminishes, there is an intermediate stage that the eddy stress ($\bar{S}$) and the Hadley cell in the southern subtropics recover in the ensemble mean time series (see Figure 6, as described in Section 3.2.1). We suspect this intermediate stage can be explained by the feedback among the SST gradient, the eddy stress, and the Hadley cell strength in the subtropics. The wind-evaporation-SST feedback discussed in the previous paragraph is strongest at around 25^{o}S. As a result, SST in the region warms more rapidly than other latitudes, leading to an increasing meridional SST gradient on the polar side and decreasing meridional SST gradient on the equatorward side (Figure 4). The increasing SST gradient on the polar side is accompanied by increasing eddy heat and momentum fluxes (not shown), the eddy stress ($\bar{S}$) and the southern Hadley cell thus re-strengthen (Figures 6b and 6c). The re-strengthening reduces the wind-evaporation-SST feedback and the anomalously positive meridional SST gradient eventually diminishes. The duration of the recovery stage increases with the mixed layer depth (Figure 4), supporting the role of SST.

Accepted for publication in *Journal of Climate*. DOI10.1175/JCLI-D-20-0151.1.

4. Summary and Discussion

The atmospheric circulation responses to extratropical thermal forcing are investigated using GFDL AM2.1 coupled to a mixed layer ocean, through an analysis of the transient responses to an abrupt imposition of the forcing. Our result suggests two distinct stages of the response (as demonstrated in Figure 10).

(a) Stage 1: Hadley cell in the forced hemisphere weakens

Surface temperature in the forced region increases after the surface heating in the Southern Hemisphere high latitudes is imposed. The imposed high latitude heating decreases meridional temperature gradient and boundary-layer stability in midlatitudes and subtropics, leading to a reduction of both eddy heat flux and momentum flux (Figure 10c). The southern cell thus weakens to balance the reduction of eddy momentum flux divergence in the subtropics (Figure 10a). The anomalous Hadley circulation is limited to the Southern Hemisphere in this stage, and there is very little change in tropical SST and precipitation (Figure 10g). While the idea of extratropical eddy influencing the strength of Hadley cell is not new, the causal relationship is clearer in our simulations compared with previous studies. For studies investigating seasonal cycles (i.e. Bordoni and Schneider 2010), the insolation in the tropics varies, therefore,

Accepted for publication in *Journal of Climate*. DOI10.1175/JCLI-D-20-0151.1.

it is difficult to identify the root cause for variation of local Rossby number and thus the abrupt transition of the monsoon circulations. Similarly, the positive correlation between Hadley cell strength and eddy stress demonstrated in Caballero (2008) among a group of global climate models does not indicate a causal relationship. In our simulations, the imposed extratropical forcing is the root cause of all of the responses. In addition, the time-scale for Stage 1 responses is independent of mixed layer depth (Figure 5), supporting the interpretation that this stage being controlled by atmospheric momentum flux changes.

(b) Stage 2: cross-equatorial Hadley cell responses

The reduction of eddy momentum flux divergence in Stage 1 also leads to decreasing easterly trades at the surface (Figure 10e), reducing evaporation and resulting in warmer SST in the SH subtropics. Once the anomalous warming propagates to deep tropics and the inter-hemispheric temperature gradient becomes significant, an anomalous cross-equatorial cell develops and the tropical precipitation shifts southward (Figures 10b, 10f, 10h). The cross-equatorial cell is confined in the deep tropics, where angular momentum is nearly constant. Once developed, the anomalous cross-equatorial cell is an order of magnitude stronger than the anomalous Hadley circulation in Stage

Accepted for publication in *Journal of Climate*. DOI10.1175/JCLI-D-20-0151.1.

1. The larger signal-to-noise ratio in the second stage may explain why the energetic framework has more support in the literature than the momentum perspective. The equilibrium responses are qualitatively similar to the responses in Stage 2. The momentum balance of the equilibrium responses can be explained by the momentum advection of the cross-equatorial Hadley cell – the Hadley cell and the eddy stress weaken in southern tropics and strengthen in northern tropics. The response time-scale of the anomalous cross-equatorial cell is roughly proportional to mixed layer depth (Figure 5), suggesting the critical roles of air-sea interactions and boundary layer processes in triggering the cross-equatorial cell. The necessity of using the thermodynamic perspective to explain the anomalous Hadley cell strength in the deep tropics is consistent with Singh et al. 2017. Through comparing two idealized simulations with and without large-scale eddies, they suggested the upper layer eddy momentum flux may affect boundary layer entropy (and thus the strength of Hadley cell) by inducing a low-level frictional flow that reduces the ability of the Hadley cell to transport heat poleward.

The particular model configuration employed in our study was key to revealing the complex transient evolutions of the extratropical-to-tropical teleconnection. This is

Accepted for publication in *Journal of Climate*. DOI10.1175/JCLI-D-20-0151.1.

unlike the tropical-to-extratropical teleconnection, whose pathway and time-scale could be understood via anomalous stationary planetary wave propagation generated from Rossby wave sources resulting from convective changes in the tropical Pacific (Wallace and Gutzler 1981; Hoskins and Karoly 1981). Once developed, the planetary scale stationary wave patterns are steady, unless there are variations in background wind. The two-stage transient evolution of the tropical responses to extratropical thermal forcings reported in our study might be less relevant for a single tropical weather event triggered by extratropical perturbation. They could be, however, crucial for understanding the decadal variabilities or the transient evolution of anthropogenically forced climate change in the tropics. For transient climate responses, i.e. 1% increase CO_2 or standard RCP forcing scenarios, it is likely that mechanisms with various time-scales all playing a role in shaping the forced responses.

Our experimental setup and a large number of ensemble members allow us to reveal the two-stage mechanisms operating in the inter-annual time-scale that are not represented in simplified models with fixed SST (or relaxing toward an equilibrium SST), while isolating the roles of stationary waves and ocean dynamics. A more careful

Accepted for publication in *Journal of Climate*. DOI 10.1175/JCLI-D-20-0151.1.

and systematic evaluation of the magnitudes and time-scales of various mechanisms through a hierarchy of numerical models of the atmosphere-ocean-land system is important to obtain a full picture understanding of extratropical influences on tropical climate. Some open questions that can be addressed using models with different complexity include:

(1) The influence of seasonality: Eddies are stronger in the winter hemisphere. However, the influence of eddy momentum flux may be more apparent for the weak summer Hadley cell in the subtropics, where the Rossby number is small and the Hadley cell is closer to an eddy-driven regime (Eq. 1.1; Kang and Lu 2012). It is yet to be explored how would the time-scales for the two stages vary in simulations with seasonally varying insolation.

(2) The influence of zonal asymmetry: In our zonally symmetric aquaplanet model, the surface boundary is covered by a uniform mixed layer ocean. The eddy-mean flow interactions may be damped by the large thermal inertia of the mixed layer ocean, as the mean circulation is strongly constrained by SST. In a more realistic configuration, the small heat capacity of landmasses and the shallow mixed layer depth in the eastern oceanic basins may allow stronger feedback

Accepted for publication in *Journal of Climate*. DOI10.1175/JCLI-D-20-0151.1.

between eddy momentum flux and regional mean circulations, which then strengthen the responses in the momentum-driven stage (Stage 1). In addition, including zonal asymmetry also induces zonal variations of storm tracks and eddy momentum flux, allowing eddies to affect local Hadley cell. The wind-evaporation-SST mechanism may be more concentrated in the eastern basins, where the climatological trades are more organized and the mixed layer depth is shallower, altering the time-scale of the tropical responses.

(3) The influence of dynamical ocean: We have not considered the role of the dynamical ocean, which is reported to damp the tropical atmospheric circulation responses in many recent studies (Deser et al. 2015; Kay et al. 2016; Tomas et al. 2016; Hawcroft et al. 2017; Kang et al. 2018). While we do not expect changes in ocean dynamics playing critical roles for Stage 1 responses, the time-scale of the cross-equatorial Hadley cell response may be affected by the damping mechanism of Ekman transport (Schneider 2014, Green and Marshall 2017, Kang et al. 2018). Through investigating responses in long simulations (more than 50 years) in fully coupled models, Wang et al. (2018), Lin (2020), and Kang et al. (2020) further suggest a hemispherically symmetric

Accepted for publication in *Journal of Climate*. DOI10.1175/JCLI-D-20-0151.1.

Hadley cell response emerge as some oceanic processes affect SST along the cold tongue, potentially overwhelming the Stage 2 cross-equatorial cell responses in decadal time-scales.

Accepted for publication in *Journal of Climate*. DOI 10.1175/JCLI-D-20-0151.1.

Acknowledgments

We sincerely thank Prof. LinHo for his encouragements and constructive inputs. YTH, HYT, YJC were supported by Ministry of Science and Technology of Taiwan (MOST 109-2636-M-002-011- and MOST 106-2923-M-002-007-MY2). S.M.K. was supported by Basic Science Research Program through the National Research Foundation of Korea (NRF) funded by the Ministry of Science, ICT and Future Planning (2019R1F1A1063392). Outputs from our AM2 simulations and figure codes are publicly available at https://doi.org/10.6084/m9.figshare.12978476

Accepted for publication in *Journal of Climate*. DOI 10.1175/JCLI-D-20-0151.1.

Appendix

Changes in wave activities

Section 3.2.1 explains changes in eddy momentum flux divergence ($\delta\bar{S}$) in the subtropics via E-P flux. Here, we investigate factors contributing to variations in E-P flux.

The initial warming in the forced region weakens the climatological pattern of eddy heat and momentum flux, as indicated by the downward pointing arrows in midlatitudes and equatorward pointing arrows in subtropics. The weakening could be observed soon after imposing the forcing (before the occurrence of Stage 1) and is amplified throughout the simulations.

a. The baroclinic mechanism – a reduction of wave source

Based on Eq.2.3, the horizontal heat flux ($\overline{v'\theta'}$), the stability ($\bar{\theta}_z$), and the vertical eddy momentum flux $\overline{v'w'}$ can all influence the vertical component of E-P flux. The Imposed heating reduces the temperature gradient (blue contours in Figure A1(e)) and thus leads to the weakening of poleward eddy heat flux (red contours in Figure A1(e)). Also, the imposed heating propagates horizontally and vertically, increasing temperature at around 750hpa more than those near the surface. The lower

Accepted for publication in *Journal of Climate*. DOI10.1175/JCLI-D-20-0151.1.

tropospheric stability between 30°S~60°S increases (blue contours in Figure A1(f)). Both reducing horizontal heat flux and increasing stability contribute positivity to the reduction of the vertical component of E-P flux. The contribution from vertical eddy momentum flux is an order of magnitude smaller (not shown). We hypothesize that the reduction of baroclinicity on the equatorward side of the forcing reduces the wave source near the surface and thus decreases the momentum flux aloft. The reduction of wave sources and the associated momentum flux changes are consistent with those in global warming simulations, although the initial triggers differ (Frierson 2008; Lorenz and DeWeaver 2014).

b. The barotropic mechanism – eddy mean flow interactions

Another possible explanation for the weakening of eddy momentum flux divergence at the edge of the Hadley cell is the barotropic eddy-mean flow interaction mechanism (Chen et al. 2008; Lu et al. 2008). As shown in Figure A2, we do not find it to be the key mechanism leading to the reduction of eddy momentum flux divergence ($\bar{S}$) in the subtropics. As reviewed by Shaw (2020), the mechanism is as follow: The imposed warming modifies the meridional temperature gradient in the baroclinic zone. Through thermal wind adjustments, zonal mean zonal wind alters. The eddy

Accepted for publication in *Journal of Climate*. DOI 10.1175/JCLI-D-20-0151.1.

phase speed is expected to change, which shifts the critical latitudes (where background zonal mean zonal wind equals eddy phase speed) and affects eddy momentum flux divergence ($\bar{S}$). While imposing heating does lead to decreasing temperature gradient and reducing zonal mean zonal wind in midlatitudes in our simulation, the eddy phase speed does not change significantly. The limited influence of the background wind on the eddy phase speed is likely due to the baroclinic zone being more equatorward (around 40^{o}S) than the regions with strong background wind speed change (50^{o}S~60^{o}S). The zonal mean zonal wind changes in the subtropics are also small in Stage 1. The largest contribution of anomalous eddy momentum flux appears to arise from eddies with the phase speeds that are similar to that contribute to most of the eddy momentum flux in the control case, implying changes in eddy momentum flux may be originated from changes in eddy sources described in the baroclinic mechanism.

Accepted for publication in *Journal of Climate*. DOI10.1175/JCLI-D-20-0151.1.

References

Adam, O., T. Bischoff, and T. Schneider, 2016: Seasonal and Interannual Variations of the Energy Flux Equator and ITCZ. Part I: Zonally Averaged ITCZ Position. *Journal of Climate*, **29**, 3219-3230.

Andrews, D. G., 1987: On the interpretation of the Eliassen- Palm flux divergence. *Quarterly Journal of the Royal Meteorological Society*, *113*(475), 323-338.

Becker, E., G. Schmitz, and R. GeprÄGs, 1997: The feedback of midlatitude waves onto the Hadley cell in a simple general circulation model. *Tellus A*, **49**, 182-199.

Bordoni, S., and T. Schneider, 2008: Monsoons as eddy-mediated regime transitions of the tropical overturning circulation. *Nature Geoscience*, **1**, 515-519.

——, 2010: Regime Transitions of Steady and Time-Dependent Hadley Circulations: Comparison of Axisymmetric and Eddy-Permitting Simulations. *Journal of the Atmospheric Sciences*, **67**.

Broccoli, A., K. Dahl, and S. Ronald, 2006: Response of the ITCZ to Northern Hemisphere cooling. *Geophysical Research Letters - GEOPHYS RES LETT*, **33**.

Accepted for publication in *Journal of Climate*. DOI10.1175/JCLI-D-20-0151.1.

Caballero, R., 2007: Role of eddies in the interannual variability of Hadley cell strength. *Geophysical Research Letters*, **34**.

——, 2008: Hadley cell bias in climate models linked to extratropical eddy stress. *Geophysical Research Letters*, **35**.

Chang, P., R. Saravanan, L. Ji, and G. C. Hegerl, 2000: The Effect of Local Sea Surface Temperatures on Atmospheric Circulation over the Tropical Atlantic Sector. *Journal of Climate*, **13**, 2195-2216.

Chen, G., J. Lu, and D. M. W. Frierson, 2008: Phase speed spectra and the latitude of surface westerlies: Interannual variability and global warming trend. *Journal of Climate*, *21*(22), 5942-5959.

Chiang, J. C. H., and C. M. Bitz, 2005: Influence of high latitude ice cover on the marine Intertropical Convergence Zone. *Climate Dynamics*, **25**, 477-496.

Chiang, J. C. H., and A. R. Friedman, 2012: Extratropical Cooling, Interhemispheric Thermal Gradients, and Tropical Climate Change. *Annual Review of Earth and Planetary Sciences*, **40**, 383-412.

Accepted for publication in *Journal of Climate*. DOI10.1175/JCLI-D-20-0151.1.

Chiang, J. C. H., W. Cheng, and C. M. Bitz, 2008: Fast teleconnections to the tropical Atlantic sector from Atlantic thermohaline adjustment. *Geophysical Research Letters*, **35**.

Cvijanovic, I., and J. C. H. Chiang, 2013: Global energy budget changes to high latitude North Atlantic cooling and the tropical ITCZ response. *Climate Dynamics*, **40**, 1435-1452.

Delworth, T. L., and Coauthors, 2006: GFDL's CM2 Global Coupled Climate Models. Part I: Formulation and Simulation Characteristics. *Journal of Climate*, **19**, 643-674.

Deser, C., R. A. Tomas, and L. Sun, 2015: The Role of Ocean–Atmosphere Coupling in the Zonal-Mean Atmospheric Response to Arctic Sea Ice Loss. *Journal of Climate*, **28**, 2168-2186.

Deser, C., A. Phillips, V. Bourdette, and H. Teng, 2012: Uncertainty in climate change projections: the role of internal variability. *Climate Dynamics*, **38**, 527-546.

Dong, B.-W., and R. T. Sutton, 2002: Adjustment of the coupled ocean–atmosphere system to a sudden change in the Thermohaline Circulation. *Geophysical Research Letters*, **29**, 18-11-18-14.

Accepted for publication in *Journal of Climate*. DOI10.1175/JCLI-D-20-0151.1.

Donohoe, A., and A. Voigt, 2017: Why Future Shifts in Tropical Precipitation Will Likely Be Small: Patterns and Mechanisms. 115-137.

Frierson, D. M., 2008: Midlatitude static stability in simple and comprehensive general circulation models. *Journal of the atmospheric sciences*, *65*(3), 1049-1062.

Green, B., & J. Marshall, 2017: Coupling of trade winds with ocean circulation damps ITCZ shifts. *Journal of Climate*, *30*(12), 4395-4411.

Hawcroft, M., J. M. Haywood, M. Collins, A. Jones, A. C. Jones, and G. Stephens, 2017: Southern Ocean albedo, inter-hemispheric energy transports and the double ITCZ: global impacts of biases in a coupled model. Climate Dynamics, 48, 2279-2295.

Hill, S. A., Ming, Y., & I. M. Held, 2015: Mechanisms of forced tropical meridional energy flux change. *Journal of Climate*, *28*(5), 1725-1742.

Hoskins, B. J., and D. J. Karoly, 1981: The Steady Linear Response of a Spherical Atmosphere to Thermal and Orographic Forcing. Journal of the Atmospheric Sciences, 38, 1179-1196.

Accepted for publication in *Journal of Climate*. DOI10.1175/JCLI-D-20-0151.1.

Hwang, Y.-T., and D. M. W. Frierson, 2013: Link between the double-Intertropical Convergence Zone problem and cloud biases over the Southern Ocean. *Proceedings of the National Academy of Sciences*, **110**, 4935.

Hwang, Y.-T., D. M. W. Frierson, and S. M. Kang, 2013: Anthropogenic sulfate aerosol and the southward shift of tropical precipitation in the late 20th century. *Geophysical Research Letters*, **40**, 2845-2850.

Hwang, Y.-T., S.-P. Xie, C. Deser, and S. M. Kang, 2017: Connecting tropical climate change with Southern Ocean heat uptake. *Geophysical Research Letters,* **44**, 9449-9457.

Jia, F., and L. Wu, 2013: A Study of Response of the Equatorial Pacific SST to Doubled-CO2Forcing in the Coupled CAM-1.5-Layer Reduced-Gravity Ocean Model. *Journal of Physical Oceanography*, **43**, 1288-1300.

Kang, S. M., D. M. W. Frierson, and I. M. Held, 2009: The Tropical Response to Extratropical Thermal Forcing in an Idealized GCM: The Importance of Radiative Feedbacks and Convective Parameterization. *Journal of the Atmospheric Sciences*, **66**, 2812-2827.

Accepted for publication in *Journal of Climate*. DOI10.1175/JCLI-D-20-0151.1.

Kang, S. M., Y. Shin, and S.-P. Xie, 2018: Extratropical forcing and tropical rainfall distribution: energetics framework and ocean Ekman advection. npj *Climate and Atmospheric Science*, **1**, 20172.

Kang, S. M., I. M. Held, D. M. W. Frierson, and M. Zhao, 2008: The Response of the ITCZ to Extratropical Thermal Forcing: Idealized Slab-Ocean Experiments with a GCM. *Journal of Climate*, **21**, 3521-3532.

Kang, S. M., and J. Lu, 2012: Expansion of the Hadley cell under global warming: Winter versus summer. *Journal of Climate*, **25**, 8387-8393.

Kang, S. M., 2020: Extratropical Influence on the Tropical Rainfall Distribution. *Current Climate Change Reports*, **6**, 24-36.

Kang, S. M., S.-P. Xie, Y. Shin, H. Kim, Y.-T. Hwang, M. F. Stuecker, B. Xiang, M. Hawcroft: Walker Circulation Response to Extratropical Radiative Forcing. *Science Advances*, in revision

Kay, J. E., C. Wall, V. Yettella, B. Medeiros, C. Hannay, P. Caldwell, and C. Bitz, 2016: Global Climate Impacts of Fixing the Southern Ocean Shortwave Radiation Bias in the Community Earth System Model (CESM). *Journal of Climate*, **29**, 4617-4636.

Accepted for publication in *Journal of Climate*. DOI 10.1175/JCLI-D-20-0151.1.

Kim, H.-k., and S. Lee, 2001: Hadley Cell Dynamics in a Primitive Equation Model. Part II: Nonaxisymmetric Flow. *Journal of the Atmospheric Sciences*, **58**, 2859-2871.

Lin, Y.-C., 2020: The fast and slow components of the tropical Pacific climate response to extratropical forcings in a fully coupled model, *National Taiwan University*, master thesis

Lindzen, R. S., and S. Nigam, 1987: On the Role of Sea Surface Temperature Gradients in Forcing Low-Level Winds and Convergence in the Tropics. *Journal of the Atmospheric Sciences*, **44**, 2418-2436.

Lindzen, R. S., and A. V. Hou, 1988: Hadley Circulations for Zonally Averaged Heating Centered off the Equator. *Journal of the Atmospheric Sciences*, **45**, 2416-2427.

Lorenz, D. J., and E. T. DeWeaver, 2007: Tropopause height and zonal wind response to global warming in the IPCC scenario integrations. *Journal of Geophysical Research: Atmospheres*, *112*(D10).

Accepted for publication in *Journal of Climate*. DOI10.1175/JCLI-D-20-0151.1.

Lu, J., G. Chen, and D. M .W. Frierson, 2008: Response of the zonal mean atmospheric circulation to El Niño versus global warming. *Journal of Climate*, *21*(22), 5835-5851.

Schneider, Tapio, 2006: The general circulation of the atmosphere. *Annual Review of Earth and Planetary Sciences* 34.

Schneider, T., and S. Bordoni, 2008: Eddy-Mediated Regime Transitions in the Seasonal Cycle of a Hadley Circulation and Implications for Monsoon Dynamics. *Journal of the Atmospheric Sciences*, **65**, 915-934.

Schneider, T., T. Bischoff, and G. H. Haug, 2014: Migrations and dynamics of the intertropical convergence zone. *Nature*, **513**, 45-53.

Shaw, T. A., 2019: Mechanisms of future predicted changes in the zonal mean mid-latitude circulation. *Current Climate Change Reports*, *5*(4), 345-357.

Swann, A., I. Fung, and J. Chiang, 2011: Mid-latitude afforestation shifts general circulation and tropical precipitation. *Proceedings of the National Academy of Sciences of the United States of America*, **109**, 712-716.

Accepted for publication in *Journal of Climate*. DOI10.1175/JCLI-D-20-0151.1.

The, G. G. A. M. D. T., and Coauthors, 2004: The New GFDL Global Atmosphere and Land Model AM2–LM2 Evaluation with Prescribed SST Simulations. *Journal of Climate*, **17**, 4641-4673.

Tomas, R. A., C. Deser, and L. Sun, 2016: The Role of Ocean Heat Transport in the Global Climate Response to Projected Arctic Sea Ice Loss. *Journal of Climate*, **29**, 6841-6859.

Walker, C. C., and T. Schneider, 2006: Eddy Influences on Hadley Circulations: Simulations with an Idealized GCM. *Journal of the Atmospheric Sciences*, **63**, 3333-3350.

Wallace, J. M., and D. S. Gutzler, 1981: Teleconnections in the Geopotential Height Field during the Northern Hemisphere Winter. *Monthly Weather Review*, **109**, 784-812.

Wang, K., Deser, C., Sun, L., & R. A. Tomas, 2018: Fast response of the tropics to an abrupt loss of Arctic sea ice via ocean dynamics. *Geophysical Research Letters*, *45*(9), 4264-4272.

Accepted for publication in *Journal of Climate*. DOI10.1175/JCLI-D-20-0151.1.

Wei, H.-H., and S. Bordoni, 2018: Energetic Constraints on the ITCZ Position in Idealized Simulations With a Seasonal Cycle. *Journal of Advances in Modeling Earth Systems*.

Wei, H. H., & S. Bordoni, 2020: Energetic Constraints on the ITCZ position in the Observed Seasonal Cycle from MERRA-2 Reanalysis. *Geophysical Research Letters*, e2020GL088506.

Woelfle, M. D., C. S. Bretherton, and D. M. W. Frierson, 2015: Time scales of response to antisymmetric surface fluxes in an aquaplanet GCM. *Geophysical Research Letters*, **42**, 2555-2562.

Xie, S.-P., C. Deser, G. A. Vecchi, J. Ma, H. Teng, and A. T. Wittenberg, 2010: Global Warming Pattern Formation: Sea Surface Temperature and Rainfall. *Journal of Climate*, **23**, 966-986.

Yoshimori, M., and A. J. Broccoli, 2009: On the link between Hadley circulation changes and radiative feedback processes. *Geophysical Research Letters*, **36**.

Zhang, R., and T. L. Delworth, 2005: Simulated Tropical Response to a Substantial Weakening of the Atlantic Thermohaline Circulation. *Journal of Climate*, **18**, 1853-1860.

Accepted for publication in *Journal of Climate*. DOI10.1175/JCLI-D-20-0151.1.

Figure Caption List

Figure 1. Equilibrium responses of surface temperature, precipitation, and atmospheric circulations. (a) Latitudinal distribution of imposed forcing H (W/m^2). (b) The zonal mean SST in all heating cases. (c) Anomalous zonal wind (shaded, m/s), anomalous meridional mass streamfunction (green contours, CI = 10^{11} kg/s) in equilibrium in MLD200 case, and climatological zonal wind (black contours, CI = 15 m/s, zero contour omitted and negative dashed), and climatological E-P fluxes (vectors, m^2/s^2). (d) Same as (b), but for precipitation.

Figure 2. Equilibrium responses of circulation and momentum fluxes. Zonal mean of *S* (shaded, m/s^2) and mass streamfunction (green contours, with CI = 10^{11}kg/s, solid for positive and dashed for negative contour, and grey contours for zero) (a) in the control case, (b) in the MLD200 case, and (c) the anomalies (the MLD200 case minus control). *S* in the control case are plotted as black contours (with CI = 10^{-5} m/s^2 zero contour omitted and negative dashed) in (c) for reference.

Figure 3. Equilibrium responses of energy transports. Northward atmospheric energy transports (PW) (a) in the control case, (b) in the MLD200 case, and (c) anomalies (the MLD200 case minus control), with total MSE transport in black,

Accepted for publication in *Journal of Climate*. DOI10.1175/JCLI-D-20-0151.1.

contribution from DSE in red, contribution from moisture in blue. Note that in the range of y axes are different between (a)(b) and (c).

Figure 4. Time series of zonal mean meridional mass streamfunction and SST. Anomalous zonal mean meridional mass streamfunction at 700hPa (shaded, kg/s) and SST (grey contours, CI = 0.3 ^{o}C, zero contour omitted and negative dashed) in cases with (a) 200MLD, (b) 100MLD, and (c) 50 MLD. The vertical grey solid lines mark the start times of Stage 1 and 2. The horizontal red lines indicate the northern edge of imposed forcing. The right column shows the near-equilibrium responses.

Figure. 5. The start time of Stage 1 & 2. The start time of Stage 1 (cross) and 2 (asterisk) in MLD 200/100/50 cases.

Figure 6. Time series of Stage 1-associated responses in MLD200 case. Anomalous zonal mean (a) daily *S* (shaded, m/s^2) and daily f*v* (blue contours with CI = 5x10^{-6} 1/s^2, zero contour omitted and negative dashed) in the upper atmosphere (above 700hPa), (b) daily Southern Hemisphere Hadley cell (φ_{SH}, kg/s), (c) daily *S* above 700hPa and between 15^{o}S~25^{o}S (m/s^2), and (d) daily surface wind speed between 15^{o}S~25^{o}S (m/s). The vertical solid lines mark the start times of Stage 1 and 2. The right column shows the near-equilibrium responses. In (a), the horizontal red

Accepted for publication in *Journal of Climate*. DOI10.1175/JCLI-D-20-0151.1.

line indicates the northern edge of imposed forcing and the horizontal grey lines mark the latitude of 0.4 local Rossby number. The thick black lines in (b)~(d) indicate the ensemble mean, with each ensemble in grey. Note that in (c), the range of y axes are different between the left and right panel. The time series are smoothed by 15-day running mean to remove high frequency internal variability.

Figure 7. Time series of Stage 2-associated responses in MLD200 case. Anomalous zonal mean (a) northward MSE transport (shaded, PW), SST (grey contours with CI = 0.3 ^{o}C, zero contour omitted and negative dashed), and anomalous precipitation (contour = 1, 2, 4, 8, 16 mm/day, positive purple and negative green), (b) daily cross-equatorial Hadley cell index ($\varphi_{EQ},$ (kg/s), (c) daily interhemispheric asymmetric SST index ($\Delta_{SST,}$ ^{o}C), and (d) energy flux equator (EFE, ^{o}). The vertical solid lines mark the start times of Stage 1 and 2. The right column shows the near-equilibrium responses. The horizontal red line in (a) indicates the northern edge of imposed forcing. The thick black lines in (b)~(d) indicate the ensemble mean, with each ensemble in light grey. Note that in (b)~(d), the range of y axes are different between the left and right panels. The time series of daily data are smoothed by 15-day running mean to remove high frequency internal variability.

Accepted for publication in *Journal of Climate*. DOI 10.1175/JCLI-D-20-0151.1.

Figure 8. WES feedback. (a) Mixed layer energy budget attribution in sourthern tropical region (between the equator and the southern edge of the Hadley cell in the SH, 27^{o}S) during Stage 1 period. The errorbars mark the one standard deviation departure from the ensemble mean of each variable. Anomalous (b) surface latent heat flux due to wind change (W/m^2) and (c) surface shortwave flux (W/m^2) in SH tropical region. The vertical dashed lines in (b) and (c) mark the start times of Stage 1 and 2, respectively. The right column shows the near-equilibrium responses. The thick black lines in (b)~(c) indicate the ensemble mean, with each ensemble in light grey.

Figure 9. Schematic diagram of the two-stage response. The upper panel shows the anomalous mass stream function at 700 hPa (shaded, power of 10 kg/s), anomalous *S* over 700hPa (light blue contours, CI = 10^{-6} m/s^2), and northward DSE transport anomaly (brown contours, CI = 0.5 PW). The lower panel shows the latent heat anomaly due to wind change (shaded, W/m^2), SST anomaly (yellow contours, CI = 0.3K), and northward moisture transport anomaly (brown contours, energy equivalent, CI = 0.5 PW, zero and positive are omitted). The blue and orange contours in vertical panels show the anomalous mass streamfunction in two stages respectively (CI = 3×10^{9} (left) and 2.4×10^{10} (right) kg/s).

Accepted for publication in *Journal of Climate*. DOI 10.1175/JCLI-D-20-0151.1.

Figure 10. Two-stage responses of the MLD200 case. (a) Anomalous zonal wind (shaded, m/s), anomalous meridional mass stream function (green contours, with CI = 3×10^9 kg/s, zero contour omitted and negative dashed), and local absolute angular momentum (grey contours, with CI = $\omega a^2/10$, ω is the angular speed, and a is the radius of the Earth), (c) anomalous S (shaded, m/s^2) and E-P flux (vector, m^2/s^2), (e) anomalous zonal mean zonal wind (m/s, plotted in blue) and meridional wind (m/s, plotted in red), climatological zonal mean zonal wind (m/s, plotted in light blue) and meridional wind (m/s, plotted in light red), and (g) anomalous zonal mean precipitation (mm/day, plotted in blue) and surface temperature (^{o}C, plotted in red) in Stage 1. (b)(d)(f)(h) are same as (a)(c)(e)(g), but for Stage 2. The CI of green contours in (b) is $1.2\text{x}10^{10}$ kg/s, which is much larger than that in (a). The Stage 1 responses refer to the differences between the average of the time period between the two start dates of Stage 1 and 2 and the climatology. The Stage 2 responses are defined as the differences between the average of the first year after the start date of Stage 2 and the average of the time period between the two start dates of Stage 1 and 2.

Figure A1. Responses of E-P flux and its divergence. Climatological E-P flux (arrows), divergence of E-P flux (shading, m/s^2), vertical gradient of potential

Accepted for publication in *Journal of Climate*. DOI10.1175/JCLI-D-20-0151.1.

temperature (blue contours, K/m, with IC = 0.001 , zero contour bolded and negative dashed), (a) eddy heat flux (red contours in left panel, Km/s, with IC = 2) and (b) meridional gradient of potential temperature (red contours, K/m, with IC = 40).

Anomalous E-P flux, divergence of E-P flux, vertical gradient of potential temperature (blue contours, K/m, with IC = 0.0001), (c) eddy heat flux (red contours in left panel, Km/s, with IC = 1) and (d) meridional gradient of potential temperature (red contours, K/m, with IC = 1). (e)-(h) as in (c)-(d) but (e)-(f) in Stage 1 and (g)-(h) in Stage 2.

Figure A2. Responses of zonal wind and eddy momentum flux. Zonally average zonal wind at 300hPa divided by cosθ (heavy lines, m/s, solid line is climatology and dashed line is ensemble mean of the MLD200 heating case), climatological (shading, m^2/s^2) and anomalous (contours, with CI = 0.05 m^2/s^2, zero contour omitted and negative dashed) eddy momentum flux in Stage 1 at 300hPa. The hatching denotes the significance at 95% confidence level.

Accepted for publication in *Journal of Climate*. DOI10.1175/JCLI-D-20-0151.1.

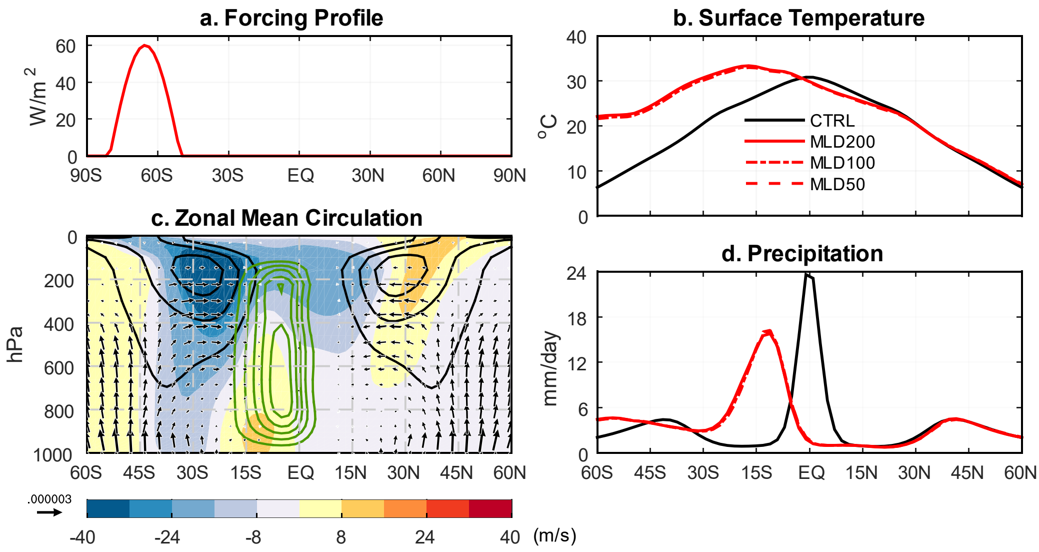

Figure 1. Equilibrium responses of surface temperature, precipitation, and atmospheric circulations. (a) Latitudinal distribution of imposed forcing H (W/m^2). (b) The zonal mean SST in all heating cases. (c) Anomalous zonal wind (shaded, m/s), anomalous meridional mass streamfunction (green contours, CI = 10^{11} kg/s) in equilibrium in MLD200 case, and climatological zonal wind (black contours, CI = 15 m/s, zero contour omitted and negative dashed), and climatological E-P fluxes (vectors, m^2/s^2). (d) Same as (b), but for precipitation.

Accepted for publication in *Journal of Climate*. DOI 10.1175/JCLI-D-20-0151.1.

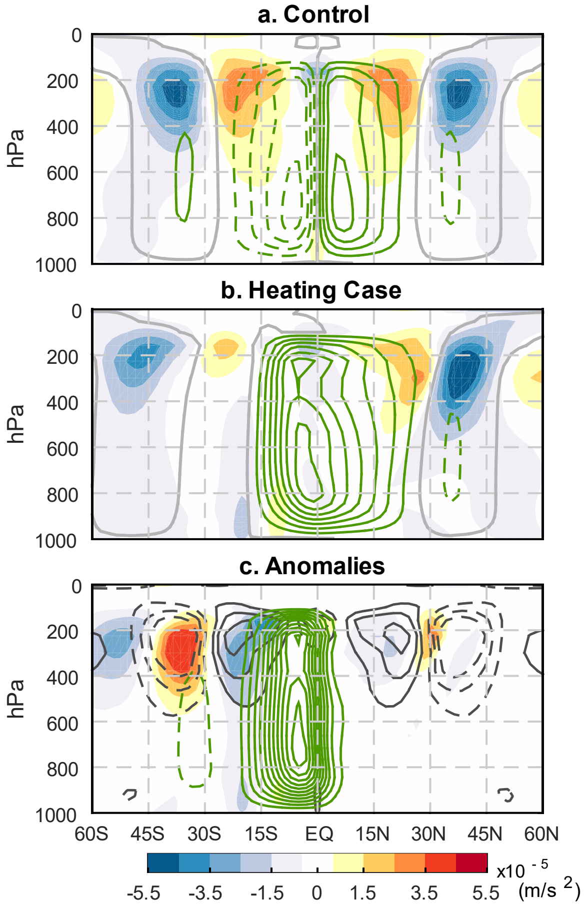

Figure 2. Equilibrium responses of circulation and momentum fluxes. Zonal mean of *S* (shaded, m/s^2) and mass streamfunction (green contours, with CI = 10^{11}kg/s, solid for positive and dashed for negative contour, and grey contours for zero) (a) in the control case, (b) in the MLD200 case, and (c) the anomalies (the MLD200 case minus control). *S* in the control case are plotted as black contours (with CI = 10^{-5} m/s^2 zero contour omitted and negative dashed) in (c) for reference.

Accepted for publication in *Journal of Climate*. DOI 10.1175/JCLI-D-20-0151.1.

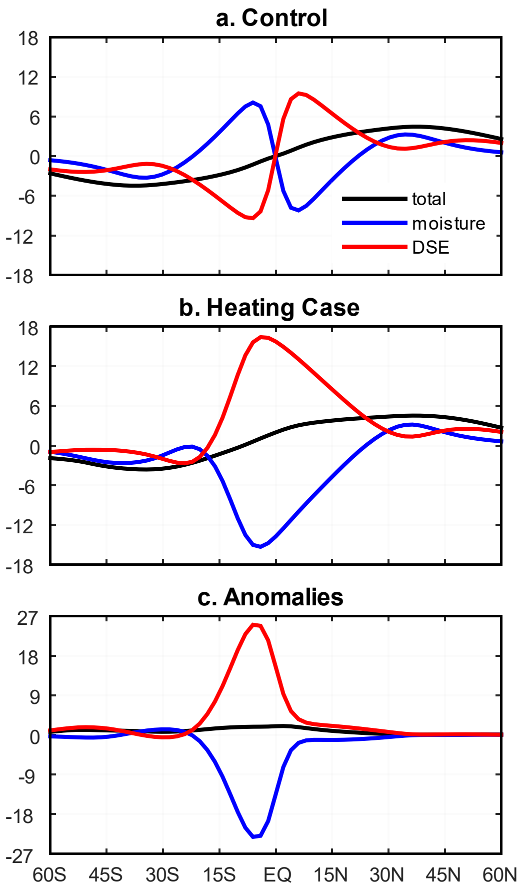

Figure 3. Equilibrium responses of energy transports. Northward atmospheric energy transports (PW) (a) in the control case, (b) in the MLD200 case, and (c) anomalies (the MLD200 case minus control), with total MSE transport in black, contribution from DSE in red, contribution from moisture in blue. Note that in the range of y axes are different between (a)(b) and (c).

Accepted for publication in *Journal of Climate*. DOI 10.1175/JCLI-D-20-0151.1.

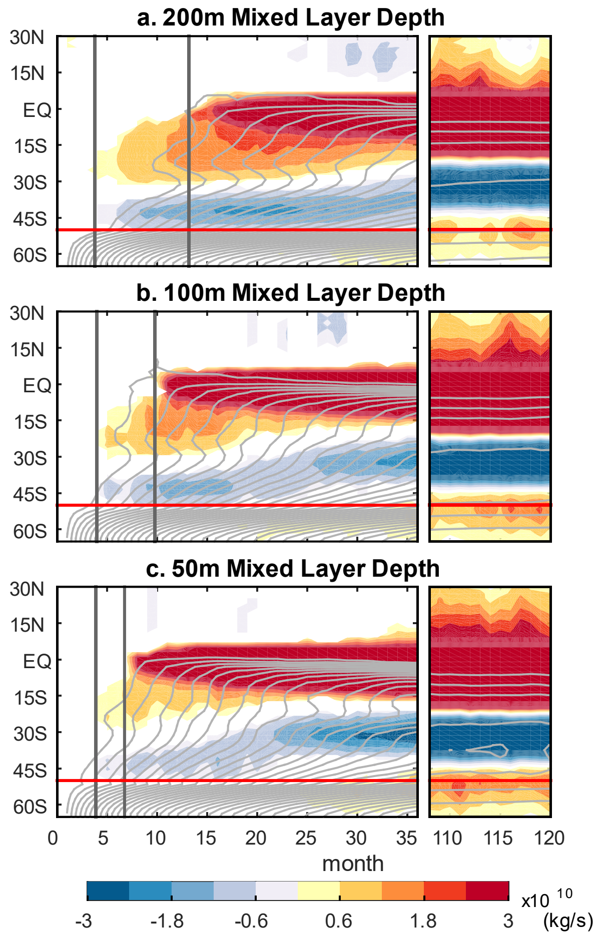

Figure 4. Time series of zonal mean meridional mass streamfunction and SST.

Anomalous zonal mean meridional mass streamfunction at 700hPa (shaded, kg/s) and SST (grey contours, CI = 0.3 °C, zero contour omitted and negative dashed) in cases with (a) 200MLD, (b) 100MLD, and (c) 50 MLD. The vertical grey solid lines mark the start times of Stage 1 and 2. The horizontal red lines indicate the northern edge of imposed forcing. The right column shows the near-equilibrium responses.

Accepted for publication in *Journal of Climate*. DOI 10.1175/JCLI-D-20-0151.1.

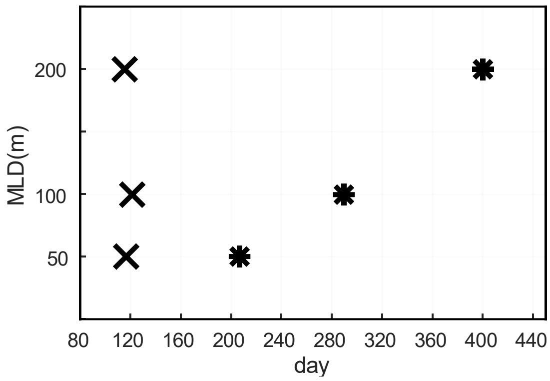

Figure. 5. The start time of Stage 1 & 2. The start time of Stage 1 (cross) and 2 (asterisk) in MLD 200/100/50 cases.

Accepted for publication in *Journal of Climate*. DOI 10.1175/JCLI-D-20-0151.1.

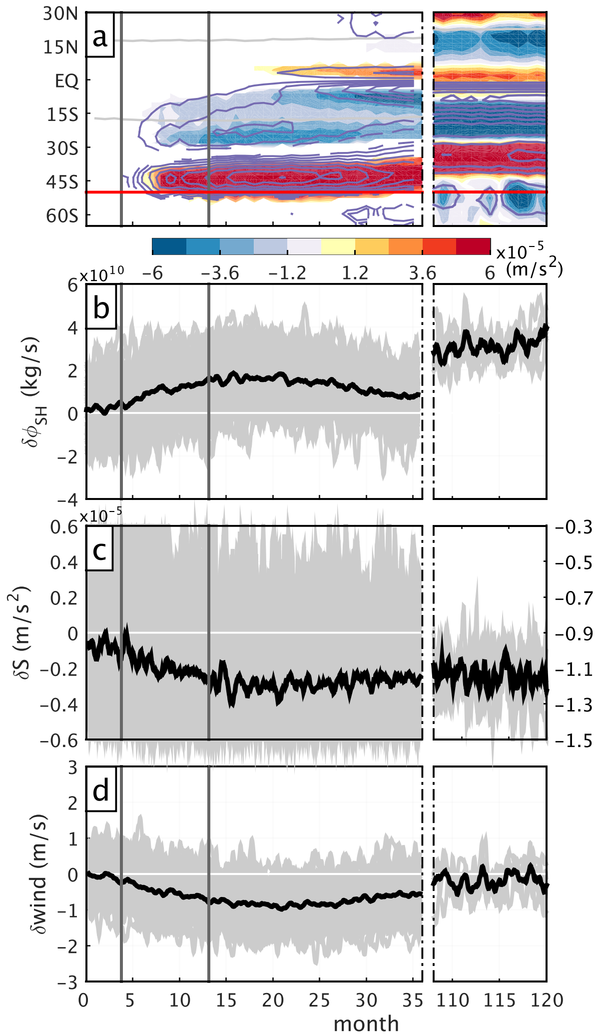

Figure 6. Time series of Stage 1-associated responses in MLD200 case.

Anomalous zonal mean (a) daily *S* (shaded, m/s^2) and daily f*v* (blue contours with CI = 5x10^{-6} 1/s^2, zero contour omitted and negative dashed) in the upper atmosphere (above 700hPa), (b) daily Southern Hemisphere Hadley cell (φ_{SH}, kg/s), (c) daily *S* above 700hPa and between 15^{o}S~25^{o}S (m/s^2), and (d) daily surface wind speed between 15^{o}S~25^{o}S (m/s). The vertical solid lines mark the start times of Stage 1 and 2. The right column shows the near-equilibrium responses. In (a), the horizontal red

Accepted for publication in *Journal of Climate*. DOI 10.1175/JCLI-D-20-0151.1.

line indicates the northern edge of imposed forcing and the horizontal grey lines mark the latitude of 0.4 local Rossby number. The thick black lines in (b)~(d) indicate the ensemble mean, with each ensemble in grey. Note that in (c), the range of y axes are different between the left and right panel. The time series are smoothed by 15-day running mean to remove high frequency internal variability.

Accepted for publication in *Journal of Climate*. DOI 10.1175/JCLI-D-20-0151.1.

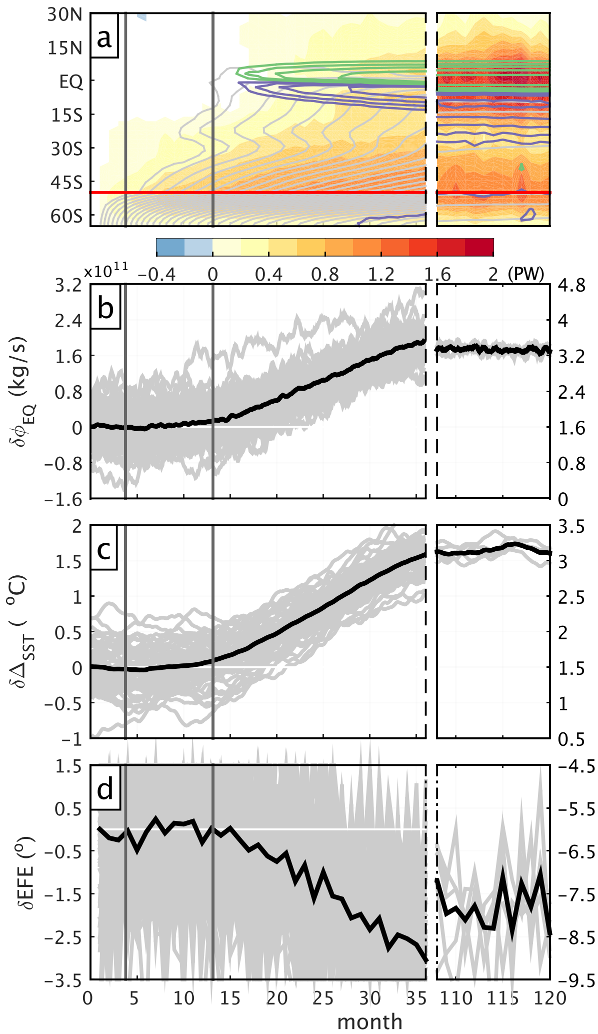

Figure 7. Time series of Stage 2-associated responses in MLD200 case.

Anomalous zonal mean (a) northward MSE transport (shaded, PW), SST (grey contours with CI = 0.3 °C, zero contour omitted and negative dashed), and anomalous precipitation (contour = 1, 2, 4, 8, 16 mm/day, positive purple and negative green), (b) daily cross-equatorial Hadley cell index (φ_{EQ}, (kg/s), (c) daily interhemispheric asymmetric SST index ($\Delta_{SST,}$ °C), and (d) energy flux equator (EFE, °). The vertical solid lines mark the start times of Stage 1 and 2. The right column shows the near-

Accepted for publication in *Journal of Climate*. DOI 10.1175/JCLI-D-20-0151.1.

equilibrium responses. The horizontal red line in (a) indicates the northern edge of imposed forcing. The thick black lines in (b)~(d) indicate the ensemble mean, with each ensemble in light grey. Note that in (b)~(d), the range of y axes are different between the left and right panels. The time series of daily data are smoothed by 15-day running mean to remove high frequency internal variability.

Accepted for publication in *Journal of Climate*. DOI10.1175/JCLI-D-20-0151.1.

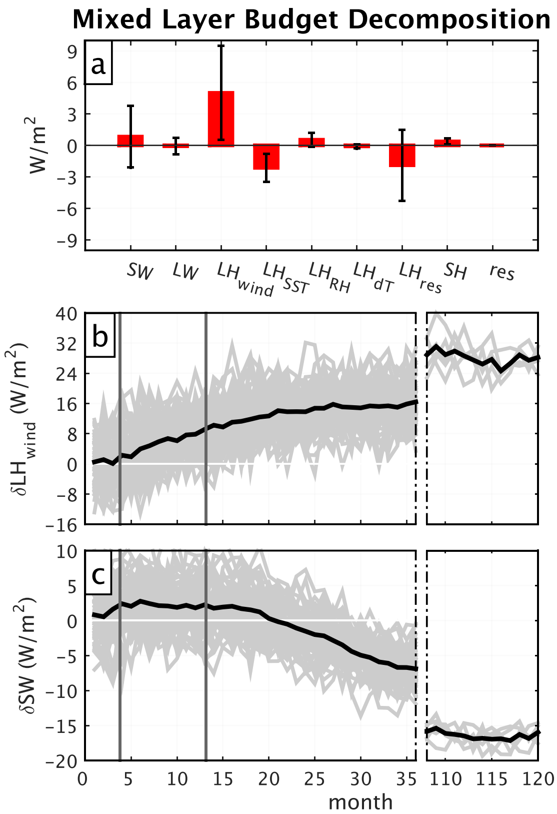

Figure 8. WES feedback. (a) Mixed layer energy budget attribution in sourthern tropical region (between the equator and the southern edge of the Hadley cell in the SH, 27^{o}S) during Stage 1 period. The errorbars mark the one standard deviation departure from the ensemble mean of each variable. Anomalous (b) surface latent heat flux due to wind change (W/m^2) and (c) surface shortwave flux (W/m^2) in SH tropical region. The vertical dashed lines in (b) and (c) mark the start times of Stage 1 and 2, respectively. The right column shows the near-equilibrium responses. The thick black lines in (b)~(c) indicate the ensemble mean, with each ensemble in light grey.

Accepted for publication in *Journal of Climate*. DOI 10.1175/JCLI-D-20-0151.1.

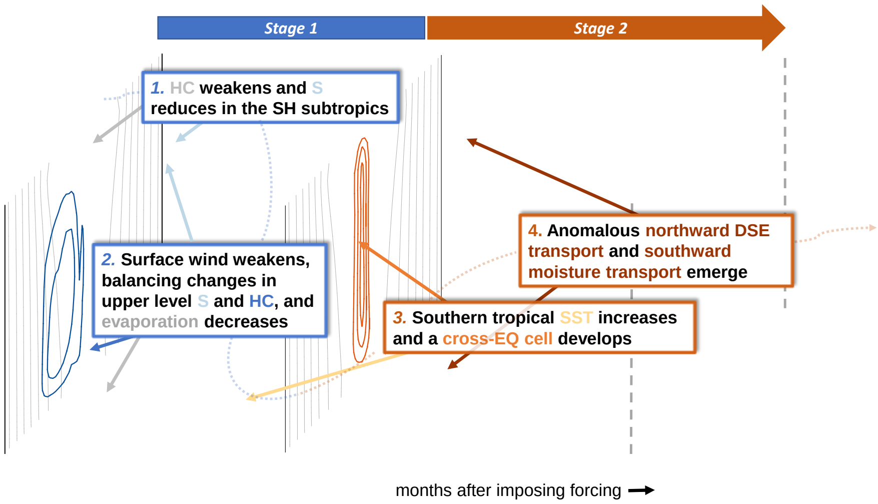

Figure 9. Schematic diagram of the two-stage response. The upper panel shows the anomalous mass stream function at 700 hPa (shaded, power of 10 kg/s), anomalous *S* over 700hPa (light blue contours, CI = 10^{-6} m/s^2), and northward DSE transport anomaly (brown contours, CI = 0.5 PW). The lower panel shows the latent heat anomaly due to wind change (shaded, W/m^2), SST anomaly (yellow contours, CI = 0.3K), and northward moisture transport anomaly (brown contours, energy equivalent, CI = 0.5 PW, zero and positive are omitted). The blue and orange contours in vertical panels show the anomalous mass streamfunction in two stages respectively (CI = 3×10^9 (left) and 2.4×10^{10} (right) kg/s).

Accepted for publication in *Journal of Climate*. DOI 10.1175/JCLI-D-20-0151.1.

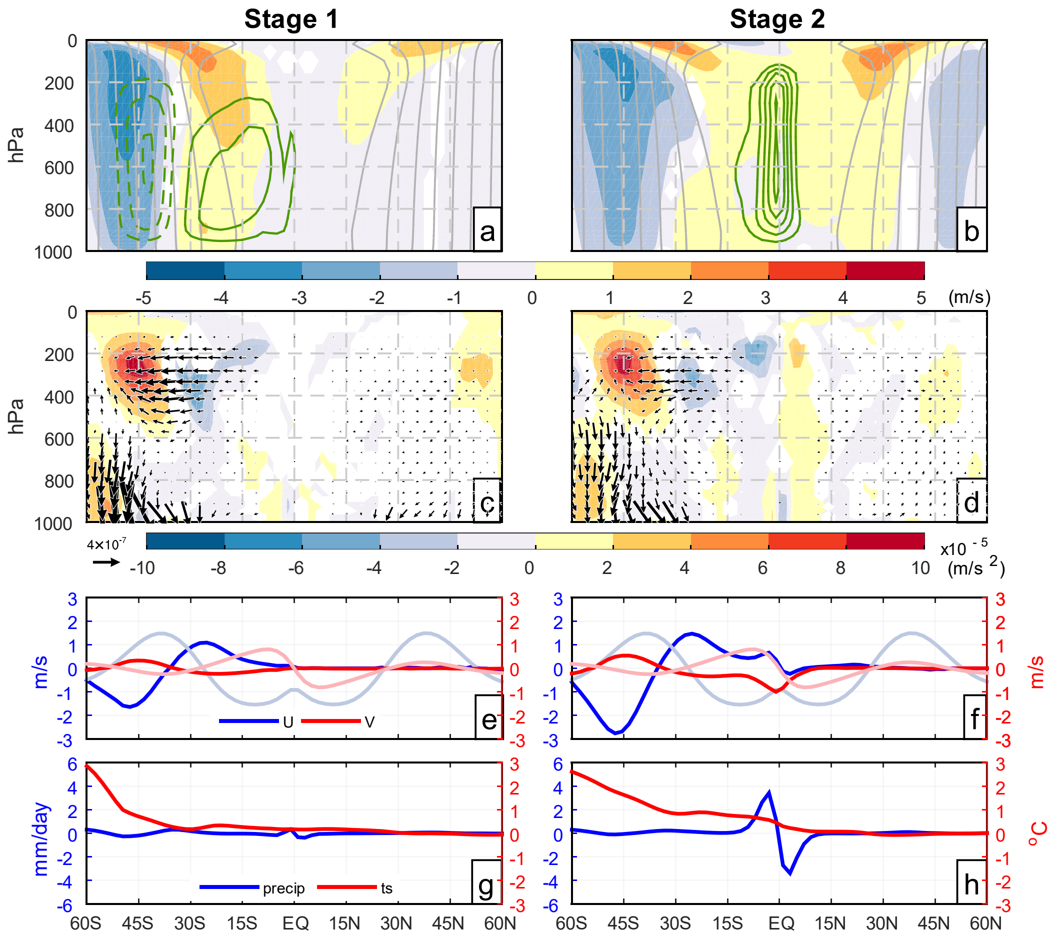

Figure 10. Two-stage responses of the MLD200 case. (a) Anomalous zonal wind (shaded, m/s), anomalous meridional mass stream function (green contours, with CI = 3×10^9 kg/s, zero contour omitted and negative dashed), and local absolute angular momentum (grey contours, with CI = $\omega a^2/10$, ω is the angular speed, and a is the radius of the Earth), (c) anomalous S (shaded, m/s^2) and E-P flux (vector, m^2/s^2), (e) anomalous zonal mean zonal wind (m/s, plotted in blue) and meridional wind (m/s, plotted in red), climatological zonal mean zonal wind (m/s, plotted in light blue) and meridional wind (m/s, plotted in light red), and (g) anomalous zonal mean

Accepted for publication in *Journal of Climate*. DOI 10.1175/JCLI-D-20-0151.1.

precipitation (mm/day, plotted in blue) and surface temperature (^{o}C, plotted in red) in Stage 1. (b)(d)(f)(h) are same as (a)(c)(e)(g), but for Stage 2. The CI of green contours in (b) is 1.2x10^{10} kg/s, which is much larger than that in (a). The Stage 1 responses refer to the differences between the average of the time period between the two start dates of Stage 1 and 2 and the climatology. The Stage 2 responses are defined as the differences between the average of the first year after the start date of Stage 2 and the average of the time period between the two start dates of Stage 1 and 2.

Accepted for publication in *Journal of Climate*. DOI10.1175/JCLI-D-20-0151.1.

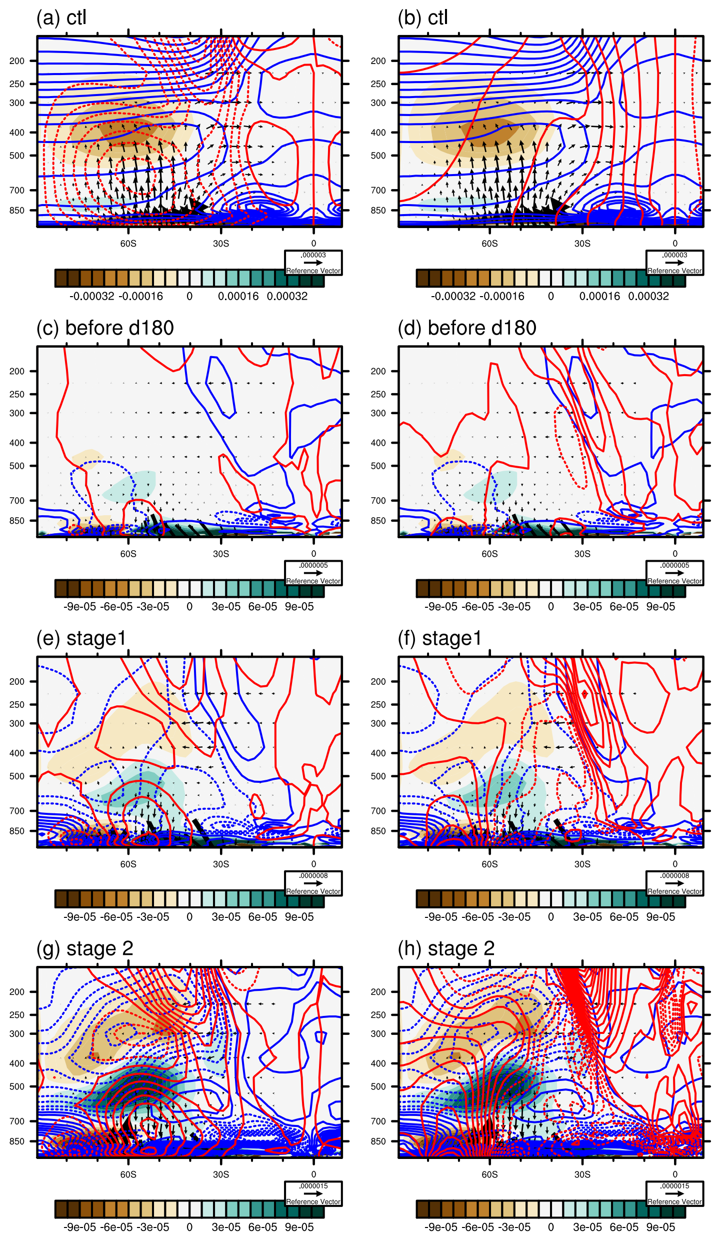

Figure A1. Responses of E-P flux and its divergence. Climatological E-P flux (arrows), divergence of E-P flux (shading, m/s^2), vertical gradient of potential temperature (blue contours, K/m, with IC = 0.001 , zero contour bolded and negative dashed), (a) eddy heat flux (red contours in left panel, Km/s, with IC = 2) and (b)

Accepted for publication in *Journal of Climate*. DOI 10.1175/JCLI-D-20-0151.1.

meridional gradient of potential temperature (red contours, K/m, with IC = 40). Anomalous E-P flux, divergence of E-P flux, vertical gradient of potential temperature (blue contours, K/m, with IC = 0.0001), (c) eddy heat flux (red contours in left panel, Km/s, with IC = 1) and (d) meridional gradient of potential temperature (red contours, K/m, with IC = 1). (e)-(h) as in (c)-(d) but (e)-(f) in Stage 1 and (g)-(h) in Stage 2.

Accepted for publication in *Journal of Climate*. DOI 10.1175/JCLI-D-20-0151.1.

.

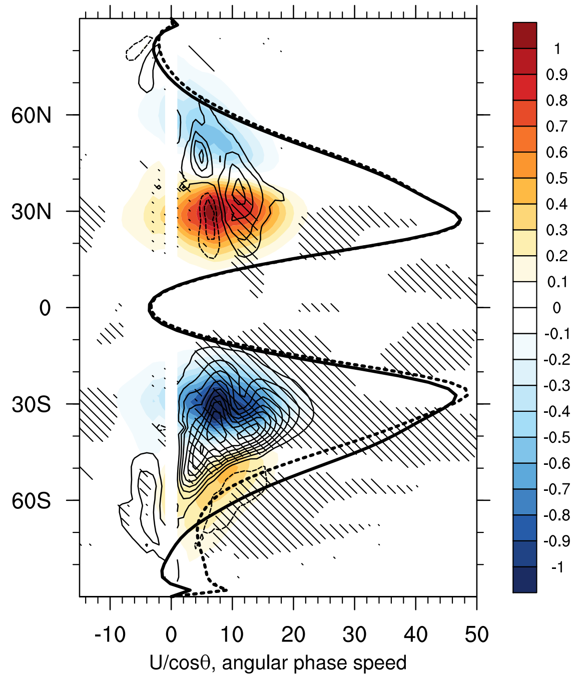

Figure A2. Responses of zonal wind and eddy momentum flux. Zonally average zonal wind at 300hPa divided by cosθ (heavy lines, m/s, solid line is climatology and dashed line is ensemble mean of the MLD200 heating case), climatological (shading, m^2/s^2) and anomalous (contours, with CI = 0.05 m^2/s^2, zero contour omitted and negative dashed) eddy momentum flux in Stage 1 at 300hPa. The hatching denotes the significance at 95% confidence level.

Accepted for publication in *Journal of Climate*. DOI 10.1175/JCLI-D-20-0151.1.